Univerzitet u Beogradu
Publikacije Elektrotehničkog Fakulteta
Serija Tehnička fizika (1998), 59–69

Envelope-function approximation for twinning superlattices in diamond-type and zinc-blende-type semiconductors

M. Tadić and Z. Ikonić

Faculty of Electrical Engineering, University of Belgrade,
P.O. Box 35-54, 11120 Belgrade, Yugoslavia

The multiband envelope-function model is extended to be able to handle twinning boundaries and more complex structures based upon it. The Hamiltonian for the mutually rotated bulk parts is set appropriately, and the effective scattering potential at the interface is modeled by a state dependent diagonal matrix δ-function potential centered at the interface. Potential strengths are fitted to the energies of bound states. Use of the method is demonstrated on the example of p-doped twinning superlattices based on germanium and gallium arsenide. The superlattice electronic structure exhibits zero energy gaps as well as folding and anticrossing behavior and agrees very well with the results of pseudopotential calculations. Intersubband optical absorption is also calculated. Each absorption peak is attributed to the specific transition, which obeys appropriate selection rule for the given polarization of the incident light. Relative magnitudes of the absorption coefficients are explained by the band structure anisotropy of germanium. Finally, it is shown that the enhanced scattering due to the symmetry removal in the twinning superlattice may bring considerable benefits in the detection of infrared light.

I Introduction

It is well established that classical superlattice states are well described by the multiband effective mass theory [1]. In addition to composite structures, where confinement is provided by the band offset, change of the atomic stacking sequence (crystal twinning) may also be employed for that purpose [2]. Structures of this kind are realized by periodic repetition of twinned layers, therefore they are appropriately called twinning superlattices (TSL's) [2]. These may be envisaged as composed of layers rotated by π rad in respect of each other about the [111] crystallographic direction. Single twinning boundaries and structures derived from them (intrinsic and extrinsic stacking faults) are among the most common dislocations in crystals, which almost always appear undesirably, and adversely affect e.g. electronic transport properties. However, the periodic array of twinning boundaries in TSL brings about coherent scattering, resulting in the appearance of miniband structure. The electronic structure

calculation of either single dislocations or TSL's normally requires microscopic methods. For instance, the self-consistent pseudopotential method was used for the electronic structure calculation of single dislocations [3], and empirical pseudopotential method (EPM) for the electronic structure and optical properties of TSL's [2, 4].

As for the possible applications of these systems, it has been known for more than a decade that systems of reduced dimensionality offer unique possibility of direct optical transitions within a single band or a few coupled bands [5]. This has had great impact on the technology of infrared detection, and applications are expected to be more diversified in forthcoming years. Among many other advantages, these detectors rely on well developed technologies of the III-V semiconductor growth and the litographic patterning. In accordance with the inverse dependence of the photoresponsivity on the effective mass, one may expect to see using only n-doped semiconductors for this purpose [6]. Yet, quantum mechanical selection rule disables the detection of normally incident light therein. This restricition is lifted in systems based on p-doped materials [7], where interaction of the electron system with in-plane polarized light is enabled by valence subbands mixing, though the responsivity is lower due to the larger effective mass. There have been a few attempts to realize these detectors, notable examples being GaAs/AlGaAs [8, 9, 10, 11, 12], InGaAs/InP [13], GaInAs/AlInAs [14], GaSb/GaAlSb [15], GaSb/InAs [16], InGaP/GaAs [17], and Si/SiGe [18, 19] two-dimensional electron gas (2DEG) structures. It was shown that theoretical results based on envelope-function theory (EFT) match quite well the experimental findings [10, 11]. Using strained systems may be beneficial [20, 21, 22], though quantum well infrared photodetectors (QWIP's) are still commonly fabricated of n-doped semiconductors, because of their superior performance. It is of interest to explore p-doped TSL's in this respect, since high intersubband absorption therein may be expected as a consequence of symmetry mismatch induced scattering, rather than by confinement by heterostructure potential. The p-like hole states are far more affected by twinning than are s-like conduction band states in a direct gap semiconductor, and clearly only the former should be explored in this respect.

Microscopic methods have, along with their advantages, some drawbacks as well. For one, it is their complexity and the associated numerical problems, which makes difficult their use for larger systems. For two, while such methods fairly succesfully predict the band structure features in the ~ 10 eV range, they may fail to reproduce accurately the fine details of the band structure in narrow energy ranges that one may be most interested in. For that reason it is useful to explore the possibility of using the envelope-function $\mathbf{k}\cdot\mathbf{p}$ method for semiconductor structures derived from twinning boundaries. This is the problem we address to in this letter. Our aim is to form the simplest, yet accurate enough model which would predict electronic and optical properties of such structures, in particular for the valence band where most interesting effects occur. An additional benefit would be a rather straightforward and physically transparent characterization of states and optical transitions among them.

The paper is organized as follows. In Sec. II the theory of electronic structure is presented and described in detail. The eigenfunctions from this part are then used in Sec. III to calculate matrix elements and the absorption coefficient. The pecalurities of the miniband structure and the dependence of absorption on light polarization and TSL parameters are discussed in Sec IV.

II Envelope-Function Theory

The structure under consideration consists of an infinite alteration of two oppositely oriented stacking sequences of n and m monolayers of a single semiconductor X(=GaAs,Ge). It may be conveniently denoted as $\mathrm{X}_n\mathrm{X}'_m$. Two subsequent half-periods may be regarded as mutually twisted by π rad about the z axis, symbolically depicted in Fig. 1 as two oppositely oriented parts. The expression we start with is a simple envelope-function equation for the manifold of eigenstates of angular momentum, arranged herein as in Ref. [1]:

$$(H + V(z))F(z) = EF(z), \tag{1}$$

where the kinetic part is given by

$$H(k_x,k_y,k_z)=\frac{\hbar^2}{2m_0}\begin{bmatrix} A_+ & B & C & 0 & \frac{1}{\sqrt{2}}B & \sqrt{2}C \\ B^\dagger & A_- & 0 & C & -\sqrt{2}Q & -\sqrt{\frac{3}{2}}B \\ C^\dagger & 0 & A_- & -B & -\sqrt{\frac{3}{2}}B^\dagger & \sqrt{2}Q \\ 0 & C^\dagger & -B^\dagger & A_+ & -\sqrt{2}C^\dagger & \frac{1}{\sqrt{2}}B^\dagger \\ \frac{1}{\sqrt{2}}B^\dagger & -\sqrt{2}Q & -\sqrt{\frac{3}{2}}B & -\sqrt{2}C & A_\Delta & 0 \\ \sqrt{2}C^\dagger & -\sqrt{\frac{3}{2}}B^\dagger & \sqrt{2}Q & \frac{1}{\sqrt{2}}B & 0 & A_\Delta \end{bmatrix}. \tag{2}$$

No strain terms are included because, with the first two nearest neighbors bond lenghts and angles

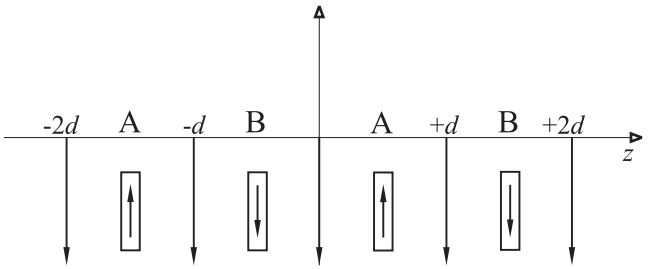

FIG. 1. Schematic view of the twinning superlattice. Two parts of the period are mutually twisted by π rad. Layer A is considered as normal with Brillouin zone k_x, k_y, and k_z axes directed along [1,1,-2], [-1,1,0], and [111] crystallographic directions, respectively. The same Hamiltonian applies to the rotated B layer, but in the coordinate system defined by unit vectors oriented in the [-1,-1,-2], [1,-1,0], and [111] directions. The interface δ-potentials are also denoted.

same as in bulk, twinning boundary is essentially strain-free [3]. This form applies to the layer with (say) the obverse orientation, and will be denoted as H_A. For the reversely oriented layer we first note that (k_x,k_y) is a good quantum number for the whole structure, so we first construct $H_A(-k_x,-k_y,k_z)$, then rotate the crystal by π rad about the z axis (cubic [111] direction), and, since rotation affects the basis states, apply the rotation matrix, which in this case reads

$$R=\mathrm{diag}(-i,+i,-i,+i,+i,-i) \tag{3}$$

to get the Hamiltonian for the reversely oriented layer

$$H_B(k_x,k_y,k_z)=RH_A(-k_x,-k_y,k_z)R^{-1} \tag{4}$$

written in the same basis and the same coordinate system as for the obversely oriented layer. We find that the diagonal matrix elements have the same form in both layers,

$$A_\pm=P\pm Q,\quad A_\Delta=P+\Delta,\quad P=\gamma_1(k_x^2+k_y^2+k_z^2),\quad Q=\gamma_3(k_x^2+k_y^2-2k_z^2), \tag{5}$$

while the off-diagonal elements in the two layers are different, and read

$$B_A=\sqrt{\frac{2}{3}}(\gamma_2-\gamma_3)(k_x+ik_y)^2-\frac{2}{\sqrt{3}}(2\gamma_2+\gamma_3)(k_x-ik_y)k_z \tag{6}$$

$$C_A=-\frac{\gamma_2+2\gamma_3}{\sqrt{3}}(k_x-ik_y)^2+2\sqrt{\frac{2}{3}}(\gamma_2-\gamma_3)(k_x+ik_y)k_z \tag{7}$$

and

$$B_B=-\sqrt{\frac{2}{3}}(\gamma_2-\gamma_3)(k_x+ik_y)^2-\frac{2}{\sqrt{3}}(2\gamma_2+\gamma_3)(k_x-ik_y)k_z \tag{8}$$

$$C_B = -\frac{\gamma_2 + 2\gamma_3}{\sqrt{3}}(k_x - ik_y)^2 - 2\sqrt{\frac{2}{3}}(\gamma_2 - \gamma_3)(k_x + ik_y)k_z. \tag{9}$$

Here k_x, k_y, and k_z denote the hole wave vector components in the coordinate system oriented along the [1,1,-2], [-1,1,0], and [1,1,1] crystallographic directions, respectively [23], γ_1, γ_2, and γ_3 are the Luttinger parameters, Δ the spin-orbit splitting, and m_0 the free electron mass. In a "heterostructure" H_A and H_B take the operator form, with $k_z \to -i\partial/\partial z$.

Single twinning boundaries and twinning superlattices are generally flat band structures, with no macroscopic potential modulation. In the vicinity of the interface, due to non-bulk-like atomic stacking sequence, the microscopic potential is different from that in bulk (the perturbation extends ~ 1 monolayer on either side of the interface [3]). As EPM indicates, this gives rise to interface bound states, which, however, cannot be found from the EFT Hamiltonian, Eqs. (1)-(7), with $V(z) = 0$. Therefore, the EFT Hamiltonian has to be amended with an appropriate short range effective interface potential, to act upon envelope functions. The simplest model potential we could devise for this purpose is the interface-centered Dirac δ-function. Calculations indicate that bound states energies found by EPM cannot be reproduced with a single δ-function, and in fact we set three δ-functions acting separately on heavy-hole (HH), light-hole (LH), and split-off (SO) bands, their strengths being determined by matching to the EPM results. This is not very unusual, unlike the microscopic potential which is unique, the macroscopic (effective) potential depends on the states it acts on. Therefore, in a single twinning boundary we have

$$V(z) = \frac{\hbar^2}{2m_0}\mathrm{diag}(V_{\mathrm{HH}}, V_{\mathrm{LH}}, V_{\mathrm{LH}}, V_{\mathrm{HH}}, V_{\mathrm{SO}}, V_{\mathrm{SO}})\delta(z), \tag{10}$$

with an appropriate (Dirac comb) generalization for TSL's. Subject to boundary conditions at interfaces and, in case of superlattices, to Bloch conditions, this Hamiltonian leads to the secular equation of the form:

$$S = \begin{bmatrix} P - R & Q \\ (P + R)E_{2\mathrm{A}}(d) & e^{i2qd}QE_{2\mathrm{B}}(-d) \end{bmatrix} \tag{11}$$

where

$$P = \begin{bmatrix} X_A & Y_A \\ D_{\mathrm{eff}}X_A + X_A G_{2\mathrm{A}}(0) & D_{\mathrm{eff}}Y_A + Y_A G_{2\mathrm{A}}(0) \end{bmatrix}, \tag{12}$$

$$R = \begin{bmatrix} 0 & 0 \\ D_\delta X_A & D_\delta Y_A \end{bmatrix}, \tag{13}$$

and

$$Q = \begin{bmatrix} -X_B & -Y_B \\ -X_B G_{2\mathrm{B}}(0) & -Y_B G_{2\mathrm{B}}(0) \end{bmatrix}, \tag{14}$$

where the capital subscripts denote respective layers, and q the superlattice wave vector. Degenerate eigenvectors corresponding to the same k_z (there are six of them in each layer) are alternately arranged as the subsequent columns of the matrices $X_{A,B}$ and $Y_{A,B}$.

We seek a solution of the system $S \cdot c = 0$ where $c = [c_A, c_B]^T$ are the coefficient of expansion of the envelope functions in the k_z modes. The matrices D_{eff} and D_δ are given in the Appendix, while $E_{2\mathrm{A}}(z)$ and $E_{2\mathrm{B}}(z)$ are given by

$$E_{2\mathrm{A}}(z) = \begin{bmatrix} E_A(z) & 0 \\ 0 & E_A(z) \end{bmatrix}, \quad E_{2\mathrm{B}}(z) = \begin{bmatrix} E_B(z) & 0 \\ 0 & E_B(z) \end{bmatrix}, \tag{15}$$

respectively, where $E_A(z)$ and $E_B(z)$ are diagonal matrices made up of the plane wave functions

$$E_{A,ij}(z) = \exp(ik_{zA,i}z)\delta_{ij} \quad E_{B,ij}(z) = \exp(ik_{zB,i}z)\delta_{ij}. \tag{16}$$

Here δ_{ij} denotes the Kronecker delta symbol. Similarly,

$$G_{2\mathrm{A}}(z) = \begin{bmatrix} G_A(z) & 0 \\ 0 & G_A(z) \end{bmatrix}, \quad G_{2\mathrm{B}}(z) = \begin{bmatrix} G_B(z) & 0 \\ 0 & G_B(z) \end{bmatrix}, \tag{17}$$

where $G_A(z)$ and $G_B(z)$ denote diagonal matrices

$$G_{A,ij}(z) = ik_{zA,i}\exp(ik_{zA,i}z)\delta_{ij}, \quad G_{B,ij}(z) = ik_{zB,i}\exp(ik_{zB,i}z)\delta_{ij}, \tag{18}$$

respectively.

It turns out that the complexity of the original problem of finding zero of the 24×24 determinant may be reduced twice if the pivoting algorithm is employed. However, in order to avoid singularities of the secular equation two such transformations should be performed. These are given by:

$$S_c \cdot c_c = \begin{bmatrix} I + iRT_qP^{-1} & QC_k \\ iQT_kQ^{-1} - QT_kQ^{-1}RT_qP^{-1} + iPT_qP^{-1} + RP^{-1} & 0 \end{bmatrix} \begin{bmatrix} c_{cA} \\ c_{cA} \end{bmatrix} = \begin{bmatrix} 0 \end{bmatrix} \tag{19}$$

and

$$S_s \cdot c_s = \begin{bmatrix} -QT_k^{-1}Q^{-1} + iQT_k^{-1}Q^{-1}RT_q^{-1}P^{-1} - PT_qP^{-1} - iRP^{-1} & 0 \\ -iI - RT_q^{-1}P^{-1} & iQS_k \end{bmatrix} \begin{bmatrix} c_{sA} \\ c_{sB} \end{bmatrix} = \begin{bmatrix} 0 \end{bmatrix}, \tag{20}$$

where C_q, S_q, C_k, S_k, T_k, and T_q are given by

$$C_q = \frac{e^{-iqd}E_{2\mathrm{A}}(d/2) + e^{iqd}E_{2\mathrm{A}}(-d/2)}{2}, \tag{21}$$

$$S_q = \frac{e^{-iqd}E_{2\mathrm{A}}(d/2) - e^{iqd}E_{2\mathrm{A}}(-d/2)}{2i}, \tag{22}$$

$$C_k = \frac{E_{2\mathrm{B}}(+d/2) + E_{2\mathrm{B}}(-d/2)}{2}, \tag{23}$$

$$S_k = \frac{E_{2\mathrm{B}}(+d/2) - E_{2\mathrm{B}}(-d/2)}{2i}, \tag{24}$$

$$T_k = C_k \cdot S_k^{-1}, \tag{25}$$

$$T_q = C_q \cdot S_k^{-1}, \tag{26}$$

respectively.

III Absorption Coefficient

The interaction Hamiltonian is obtained in the $\mathbf{A}\cdot\mathbf{v}$ gauge by finding the gradient of the hole Hamiltonian in $\mathbf{k}$ space. This matrix, which obviously has the same structure as the hole Hamiltonian, Eq. (2), may be conveniently separated into a dipole matrix and an overlap matrix [7]. A few points are worth noting here. First, HH and LH minibands are coupled by the off-diagonal matrix elements of the interaction Hamiltonian. Second, the dominant transition is provided by the dipole matrix, because of its constancy in the k_t plane. Third, the form of B and C matrix elements allows the transitions which are otherwise forbidden in composite superlattices to occur. For example, the absorption peaks for x polarized light originate from the HH→LH transitions, where one of the states is a folded one. In the composite structures, these transitions never take place, but in TSL they become possible due to the variation of dipole coupling terms in C matrix element of the interaction Hamiltonian. Finally, the transition matrix elements are furnished by the interface terms, arising from the change of sign of linear combinations of the Luttinger parameters in the C matrix element. The transition matrix element is lowered this way, though this effect is not so strong in Ge, therefore an order of magnitude higher absorption than free-carrier absorption in bulk is realized [4].

For the absorption coefficient the following expression is utilized:

$$\alpha = \frac{e^2\hbar}{8\pi^2 c\epsilon_0}\frac{1}{n\hbar\omega}\int_{-\infty}^{+\infty}dk_x\int_{-\infty}^{+\infty}dk_y\int_{-\pi/2d}^{+\pi/2d}dq\sum_i\sum_f|\frac{\hbar}{2m_0}M_{fi}|^2 \times\frac{,/2\pi}{(E_f-E_i-\hbar\omega)^2+,^2/4}(f_n(E_i)-f_n(E_f)). \tag{27}$$

Here $\hbar\omega$ denotes the photon energy, ϵ_0 the vacuum permittivity, c the speed of light, e the electron charge, n the index of refraction, , the Lorentzian full width at half maximum, f_n the Fermi-Dirac distribution function for holes, computed for the initial energy E_i and the final energy E_f, and $\hbar M_{fi}/2m_0$ denotes the transition matrix element between states i and f, obtained by summing over the four possible transitions offered by the double degeneracy of the initial and the final state. In this calculation the region of important states in the superlattice reciprocal space, bounded by planes intersecting at $(k_x,k_y,q)=(\pm0.5,\pm0.5,\pm\pi/2d)$ nm^{-1}, is subdivided into $13\times13\times17$ cubes, making up a quite fine mesh, where all the relevant states for absorption calculation are taken into account.

IV Results and Discussion

To check the validity of the model, we consider Ge and GaAs based TSL's having $n=9$ ($d=2.9$ nm) crystalline monolayers in each half period (with obverse and with reverse orientation). The reason for taking Ge is that multiple twinned ultrathin layers (though not real TSL's) have been observed in amorphized Ge films [24], and for GaAs, TSL-like structure was found in free-standing quantum wires Ref. [25]. The Luttinger parameters used in calculation are: $\gamma_1=13.35$, $\gamma_2=4.25$, $\gamma_3=5.69$ [28], and $\gamma_1=6.85$, $\gamma_2=2.10$, and $\gamma_3=2.90$ [26] in Ge and GaAs, respectively. The spin-orbit splitting energies amount to 282 meV and 340 meV, and the lattice constants are 0.56579 nm and 0.565325 nm in Ge and GaAs, respectively [26]. The EPM calculated bound states energies of a Ge single twinning boundary are -25.8 meV and -0.5 meV, corresponding to heavy and light holes, respectively, while no bound or resonant state was found in the vicinity of the SO band top. The calculated strengths of the delta potentials are $V_{\rm HH}=-2.31$ nm^{-1}, and $V_{\rm LH}=-1.08$ nm^{-1}, and $V_{\rm SO}=0$. The eigenenergies in GaAs amount to -19 meV, -0.3 meV, and -0.65 meV (relative to Δ), and the corresponding strengths of the delta potentials are $V_{\rm HH}=-1.45$ nm^{-1}, $V_{\rm LH}=-0.608$ nm^{-1}, and $V_{\rm SO}=-0.648$ nm^{-1}.

The main feature of the electronic structure that EFT predicts is the existence of zero energy gaps, i.e. the minibands folding at $k_t=\sqrt{k_x^2+k_y^2}=0$, as shown in Fig. 2. There is no effective mass reversal

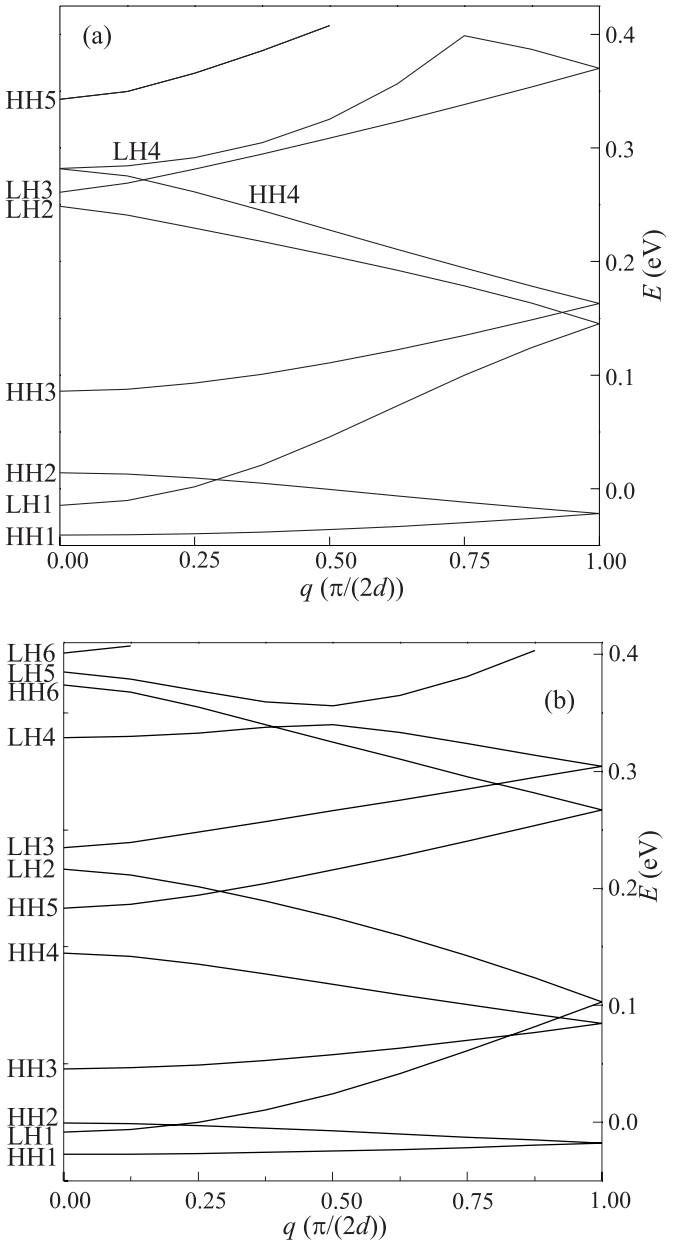

FIG. 2. The miniband dispersion in the direction of the superlattice wave vector, at $k_t = 0$ in (a) Ge twinning superlattice and (b) GaAs twinning superlattice. Numerous crossings as well as an anticrossing between LH+SO states may be noticed.

in the direction of superlattice wave vector, whereas this effect obviously occurs in the (k_x, k_y) plane, as depicted in Fig. 3. States are designated according to the bulk states dominant in the superlattice states wave function at $k_t = 0$. These are denoted in Fig. 2 as heavy-hole (HH) and light-hole (LH), the latter being a shorthand notation for the mixture of light-hole and split-off bands (LH+SO). Due to the folding effect, different effective masses, and uncoupled HH and LH+SO states, there are numerous crossings between these states in the selected energy range at $k_t = 0$, as Fig. 2 shows. As a consequence of the low effective mass of light-hole bands, the LH1+LH2 miniband is rather wide. The LH4 miniband exhibits strong anticrossing with LH5 miniband (not shown in Fig. 2(a)). Crossings at $k_t = 0$ are converted to anticrossings, and zero energy gaps disappear at finite k_t, as displayed in Fig. 3 for the superlattice wave vector $q = 0$. There exist prominent anticrossings between the first (HH1), the second (LH1), and the third (HH2) miniband. All these results are in good agreement with those obtained from EPM calculation [4]. As an example, the HH ground state energy in GaAs

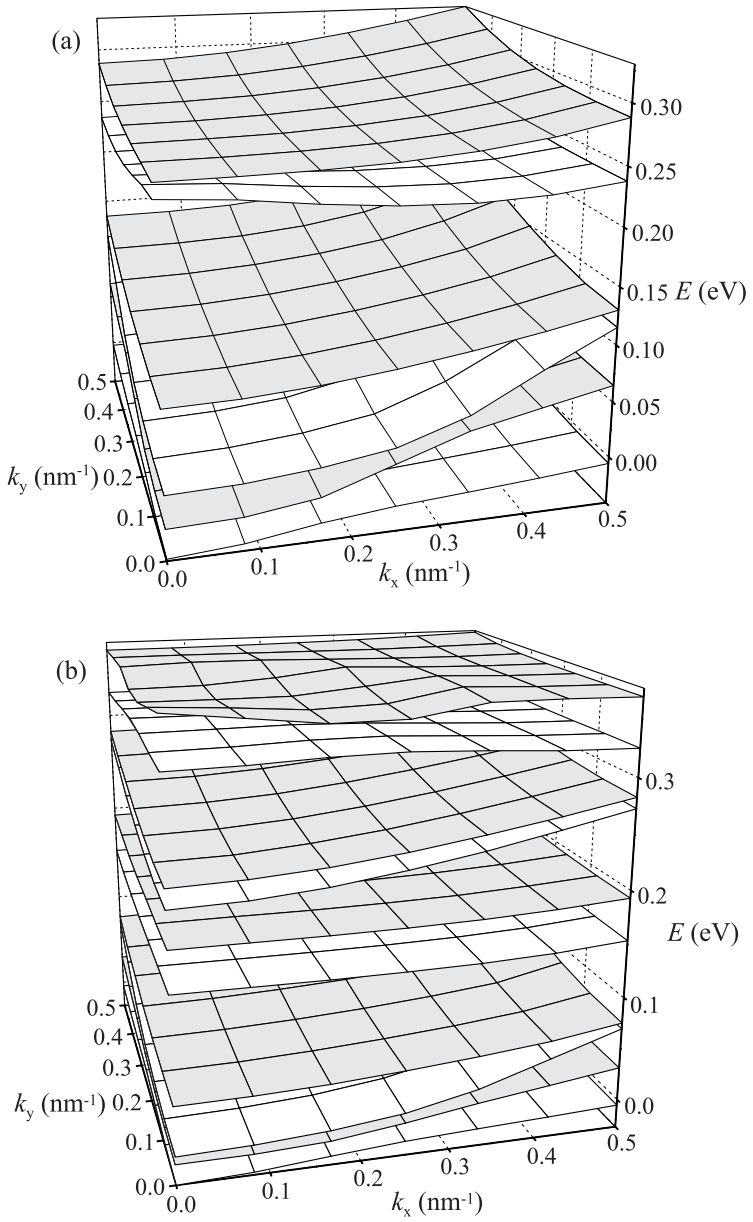

FIG. 3. In-plane miniband dispersion for $q = 0$ in (a) Ge twinning superlattice and (b) GaAs twinning superlattice. All the bands disperse in a nearly isotropic fashion, and there is a clear anticrossing between HH1 and LH1 level, and the second between LH1 and HH2 level.

is fairly well estimated by EFT, while excellent agreement between EPM and EFT was found in Ge. The discrepancy between EFT and EPM becomes negligible if the Luttinger parameters are extracted from the EPM itself, which does not seem surprising, since the fit to the dispersion relation of the EFT works best for the lowest energy states [27]. Nonetheless, we consider the deviations of the zone center energies of the order of a few meV acceptable, keeping in mind that the EPM in its different implementations (interface matching or supercell) does not really offer accuracy much better than that. Furthermore, zero energy gaps at $k_t = 0$, as well as miniband folding effect found by EPM are also yielded by EFT calculation, as clearly depicted in Fig. 3. The folding scheme is not reproduced accurately by EFT, since the hole dispersion itself is not accurately reproduced, either. In other words, eigenstates with a large superlattice wave vector are affected by the structure in a more complex way than EFT can predict.

The absorption is calculated for two polarizations of the incoming light. The ambient temperature

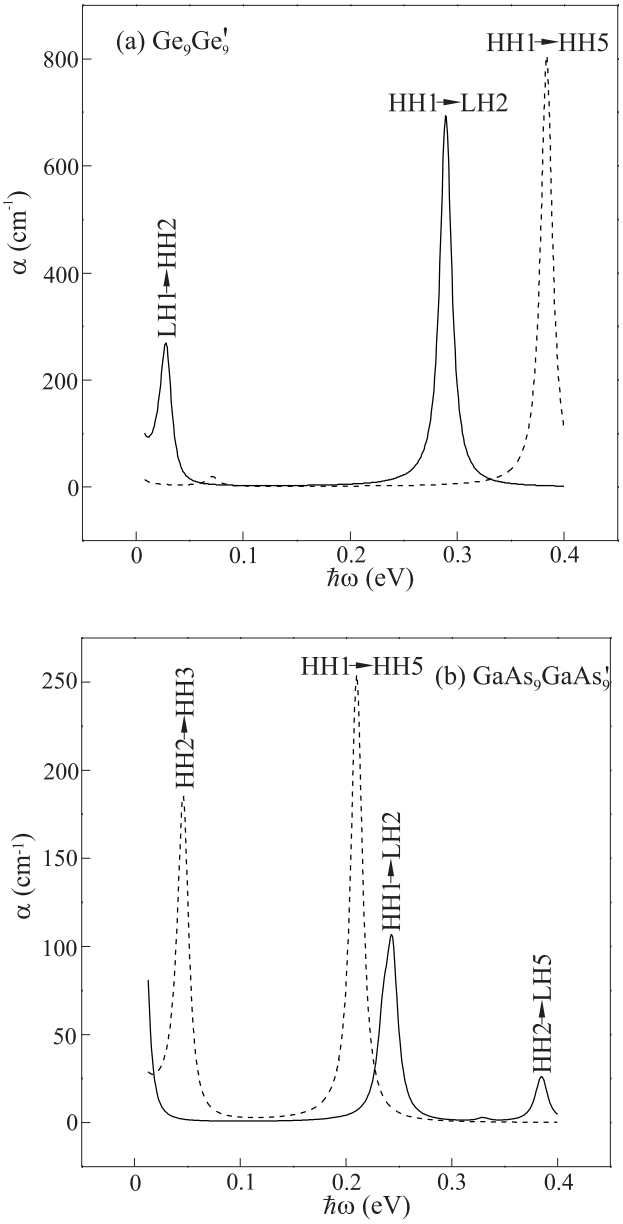

FIG. 4. The absorption spectra in (a) Ge TSL and (b) GaAs TSL for x polarized light (solid line) and for z polarized light (dashed line). The values of Luttinger parameters, bring about higher absorption for z than for x polarized light, yet the latter is of larger technological importance.

is taken to be equal to 77 K. Homogeneous doping of $N_A = 10^{17}$ cm^{-3} acceptors throughout the structure (same as in Ref. [4]) is assumed. For the homogeneous relaxation time τ =0.1 ps is adopted, corresponding to the Lorentzian width of , = 13.16 meV. The first peak of the absorption coefficient for x polarized light in Ge arises mainly from the transitions between LH1 and HH2 miniband, and occurs at 28 meV (Fig. 4(a)). The second absorption peak is shifted to much shorter wavelengths (289 meV) in the midwavelength infrared (MWIR) window, offering 2.5 times higher absorption than the first peak does. Both these transitions are enabled by the unconventional coupling mechanism between normal and folded states, as discussed above. In addition, a finite coupling arises from the effective change of the Luttinger parameters at two interfaces belonging to a superlattice period. For z polarized light the transitions between heavy-hole states take place. The single peak is located at almost the short wavelength cut-off of the MWIR window. Here again the absorption arises from the dipole interaction, but the transitions are enabled between heavy-hole states, since the coupling terms

are arranged at the main diagonal of the interaction Hamiltonian. Inter-heavy-hole matrix elements are proportional to , $_z = \gamma_1 - 2\gamma_3$, which does not vary in the structure at all, that is, there are no interface terms in the transition matrix element. This combination of the Luttinger parameters amounts to 1.05 in GaAs. The momentum matrix element between heavy and light holes is now proportional to , $_x = 2\sqrt{2/3}(\gamma_2 - \gamma_3)$, which amounts to 1.14 in GaAs. This may lead one to conclude that the absorption coefficient attains about the same value for both x polarized and z polarized light. However, this is not so because of finite contribution of the interface terms in the case of x polarization, as mentioned above. The resulting effect is about 2.5 times lower absorption of x-polarized light than of z-polarized light (Fig. 4(b)). Combinations of Luttinger parameters enabling the absorption peak for two polarizations are larger in Ge than in GaAs. For example, , $_z = 1.97$ and , $_x = 2.35$ in Ge, which implies four times stronger absorption in Ge than in GaAs. The ratio is even larger for x polarized light, due to lower interface terms in the transition matrix element.

In conclusion, the envelope-function model of the valence band electronic structure of twinning-boundary-derived semiconductor structures is devised, with crystal rotation appropriately taken into account and heuristically introduced state-dependent δ-potentials at the interface. Its appliciability and accuracy is tested on Ge-based TSL, the electronic structure and optical properties of which are calculated. The model exhibits a great deal of congruence with the pseudopotential theory. The zone-center energies as well as the dispersion curves of the lowest minibands are reproduced accurately by the method. The zero energy gaps are identified, and crossings and anticrossings are noticed and explained. Peculiar electronic structure offers coupling between otherwise forbidden states in composite superlattices. This coupling arises from the change of the off-diagonal terms of the velocity operator across the interface. It is shown that the dipole matrix elements are responsible for the absorption. The magnitude of the absorption coefficient agrees with the results of the pseudopotential theory [4], suggesting that this structure might be useful for the state-of-art quantum well infrared photodetectors. Finally, in view of considerable simplicity of this model, in contrast to microscopic approaches, it may prove useful in studying other phenomena, not only in superlattices but also in single twinning boundaries (commonly occuring defects in semiconductors, important for transport or recombination), which are the large-period limit of TLS's.

A Appendix

The boundary condition for the probability current density is obtained by integrating the system of differential equations represented by the Hamiltonian, Eq. (2), across the interface. In considerations presented in this paper there appear two matrices of the same structure as the matrix in Eq. (2) (with $\Delta \to 0$), i.e.

$$D_{eff} = D_{2B}^{-1}(D_{1A} - D_{1B}) \tag{28}$$

and

$$D_\delta = D_{2B}^{-1} V_\delta, \tag{29}$$

where D_{1A}, D_{1B}, and D_{2B} are given in Table 1.

layer	P_h	Q_h	A_+	A_-	B	C
D_{1A}	0	0	0	0	$-\frac{i}{\sqrt{3}}(2\gamma_2+\gamma_3)(k_x - ik_y)$	$i\sqrt{\frac{2}{3}}(\gamma_2-\gamma_3)(k_x+ik_y)$
D_{1B}	0	0	0	0	$\frac{i}{\sqrt{3}}(2\gamma_2+\gamma_3)(k_x - ik_y)$	$-i\sqrt{\frac{2}{3}}(\gamma_2-\gamma_3)(k_x+ik_y)$
D_{2B}	γ_1	$-2\gamma_3$	$\gamma_1 - 2\gamma_3$	$\gamma_1 + 2\gamma_3$	0	0

TABLE 1. Matrices for the probability current density derived boundary condition. These matrices are composed analogously to the hole Hamiltonian, hence the same labels are used here as in Eq. (2).

References

[1] C. Y.-P. Chao and S. L. Chuang, Phys. Rev. B **46**, 4110 (1992).

[2] Z. Ikonić, G. P. Srivastava, and J. C. Inkson, Phys. Rev. B **48**, 17181 (1993).

[3] M. Y. Chou, M. L. Cohen, S. G. Louie, Phys. Rev. B **32**, 7979 (1985).

[4] Z. Ikonić, G. P. Srivastava, and J. C. Inkson, Phys. Rev. B **52**, 14078 (1995).

[5] B. F. Levine, Semicond. Sci. Technol. **8** S400 (1993).

[6] S. R. Andrews and B. A. Miller, J. Appl. Phys. **70**, 993 (1991).

[7] Y.-C. Chang and R. B. James, Phys. Rev. B **39**, 12672 (1989).

[8] B. F. Levine, S. D. Gunapala, J. M. Kuo, S. S. Pei, and S. Hui, Appl. Phys. Lett. **59**, 1864 (1991).

[9] K. M. S. V. Bandara, B. F. Levine, and J. M. Kuo, Phys. Rev. B **48**, 7999 (1993).

[10] F. Szmulowicz and G. J. Brown, Phys. Rev. B **51**, 13203 (1995).

[11] M. Tadić and Z. Ikonić, Phys. Rev. B **52**, 8266 (1995).

[12] B. W. Kim, E. Mao, and A. Majerfeld, J. Appl. Phys. **81**, 1883 (1997).

[13] S. D. Gunapala, B. F. Levine, D. Ritter, R. Hamm, and M. B. Panish, J. Appl. Phys. **71**, 2458 (1992).

[14] H. Xie, J. Katz, and W. I. Wang, Appl. Phys. Lett. **59**, 3601 (1991).

[15] H. Xie, J. Katz, W. I. Wang, and Y. C. Chang, J. Appl. Phys. **71**, 2844 (1992).

[16] M. P. Houng, Y. H. Wang, H. H. Chen, and Y.-C. Chang, Superlatt. Microstruct. **13**, 181 (1993).

[17] H. H. Chen, Y.-H. Wang, and M.-P. Houng, IEEE J. Quantum Electron. **32**, 471 (1996).

[18] T. Fromherz, E. Koppensteiner, M. Helm, G. Bauer, J. F. Nützel, and G. Abstreiter, Phys. Rev. B **50**, 15073 (1994).

[19] T.-S. Liou, T. Wang, and C.-Y. Chang, J. Appl. Phys. **77**, 6646 (1995).

[20] S. A. Stoklitsky, P. O. Holtz, B. Monemar, Q. X. Zhao, and T. Lundström, Appl. Phys. Lett. **65**, 1706 (1994).

[21] M. Tadić and Z. Ikonić, Appl. Phys. Lett. **68**, 994 (1996).

[22] J. Chu and S. S. Li, IEEE J. Quantum Electron. **33**, 1104 (1997).

[23] Z. Ikonić, V. Milanović, and D. Tjapkin, Phys. Rev. B **46**, 4285 (1992).

[24] H. Hofmeister, A. F. Bardamid, T. Janghanns, S. A. Nepijko, Thin Solid Films **205**, 20 (1991).

[25] K. Hiruma, M. Yazawa, K. Haraguchi, K. Ogawa, J. Appl. Phys. **74**, 3162 (1993).

[26] *Semiconductors, Group IV Elements and III-V Compounds*, edited by O. Madelung, (Springer-Verlag, Berlin, 1991).

[27] D. M. Wood and A. Zunger, Phys. Rev. B **53**, 7949 (1996).

[28] J. M. Hinckley and J. Singh, Phys. Rev. B **42**, 3546 (1990).

(Received August 1998.)